Towards Molecular Conductors with a Spin-Crossover Phenomenon: Crystal Structures, Magnetic Properties and Mössbauer Spectra of [Fe(salten)Mepepy][M(dmit)$_2$] Complexes

Christophe Faulmann,*[a] Stéphane Dorbes,[a] Bénédicte Garreau de Bonneval,[a] Gábor Molnár,[a] Azzedine Bousseksou,[a] Carlos J. Gomez-Garcia,[b] Eugenio Coronado,[b] and Lydie Valade[a]

Keywords: Conducting materials / Magnetic properties / Moessbauer spectroscopy / Spin crossover / X-ray diffraction

Three new iron(III) compounds of formula [Fe(salten)-Mepepy][M(dmit)$_2$]·CH_3CN (M = Ni, Pd, Pt; H_2salten = 4-aza-heptamethylene-1,7-bis(salicylideneiminate); Mepepy = 1-(pyridin-4-yl)-2-(*N*-methylpyrrol-2-yl) ethane; dmit^{2-} = 1,3-dithiole-2-thione-4,5-dithiolato) have been synthesised and the crystal structure of each compound has been solved at different temperatures. The structures consist of alternating layers of [M(dmit)$_2$]$^-$ units and [Fe(salten)Mepepy] cations. In the Ni compound photo-isomerisation of the Mepepy ligand can be observed in dichloromethane solution. The temperature dependence of the magnetic susceptibility of the compounds reveals a gradual $S = 5/2 \rightleftharpoons S = 1/2$ spin crossover of the Fe^{III} ions. This phenomenon is confirmed by Mössbauer spectroscopy for the Ni compound, which also reveals a magnetic component at 4.5 K with a hyperfine magnetic field, H_i, of 442(3) Oe. Theoretical analysis of the thermal variation of the high-spin proportion allows us to calculate the thermodynamical parameters of the spin-crossover behaviour in this compound: energy-gap (Δ) = 1536 cm^{-1}, entropy change (ΔS) = 33 J K^{-1} mol^{-1} and a cooperative interaction, J, of 0 cm^{-1} (non-cooperative spin crossover). The fractional oxidation state complex [Fe(salten)Mepepy][Ni(dmit)$_2$]$_3$ has been obtained after electrooxidation of [Fe(salten)Mepepy]-[Ni(dmit)$_2$] in acetonitrile. It exhibits a gradual spin conversion coupled with antiferromagnetic interactions. Its room temperature electrical conductivity is 0.1 S cm^{-1}.

Introduction

Since the discovery of the organic metal TTF–TCNQ (TTF = tetrathiafulvalene; TCNQ = tetracyanoethylene) much work has been devoted to the research of new conducting systems involving either donor–acceptor complexes or fractional oxidation-state compounds. These studies resulted in the discovery of several superconductors [derived, for example, from the BEDT-TTF molecule[1] (BEDT-TTF = bis(ethylenedithio)tetrathiafulvalene) or from the M(dmit)$_2$ complex[2] (dmit^{2-} = 1,3-dithiole-2-thione-4,5-dithiolato)]. In addition, these compounds are also now being used in a new area of research by a few groups, which consists in designing hybrid materials with a combination of different physical properties such as conductivity and magnetism,[3] conductivity and optical activity,[4] or magnetism and non-linear optics.[5] The possibilities offered by this hybrid approach in the field of the molecular conductors have been highlighted very recently.[6] In this kind of materials one might either just observe coexistence between these two properties, or an interplay due to a mutual interaction between the two effects. A good example of the coexistence of properties is found in the salt β′′-(BEDT-TTF)$_4$-[Fe(ox)$_3$](H_3O)·C_6H_5CN (ox = oxalate), reported by Day and co-workers,[7] which is the first example of a paramagnetic superconductor. An interplay between conductivity and magnetism has been observed, for example, in BETS-derived complexes [BETS = bis(ethylenedithio)tetraselenafulvalene].[8] Thus, λ-[(BETS)$_2$FeCl$_4$] undergoes a metal–insulator transition at 8 K and becomes metallic again below this temperature when a magnetic field of 10 T is applied.[9] Recently, Coronado et al.[10,11] succeeded in obtaining (BEDT-TTF)$_3$[MnCr(ox)$_3$](CH_2Cl_2) and (BETS)$_3$[MnCr(ox)$_3$]-(CH_2Cl_2), which exhibit the coexistence of conductivity and ferromagnetism.

In the above-discussed complexes, each property is carried by a distinct network: the organic part is at the origin of the conductivity, due to a charge transfer or a partial oxidation state of the organic donor, whereas the inorganic part is involved in the magnetic properties. In such compounds, observation of an interplay between the properties will depend on eventual interactions between the two networks. These electronic interactions can be favoured by short contacts and/or hydrogen bonding between the ade-

[a] Laboratoire de Chimie de Coordination,
205 Route de Narbonne, 31077 Toulouse Cedex, France
E-mail: faulmann@lcc-toulouse.fr
[b] Instituto Ciencia Molecular, Universidad de Valencia
Dr. Moliner 50, 46100 Burjassot, Spain
Supporting information for this article is available on the WWW under http://www.eurjic.org or from the author.

quate molecules, although the occurrence of the desired interplay is still not controllable. An attractive way of increasing the π–d interactions between the two networks consists of connecting them by covalent linkages. This has been attempted by Ouahab and co-workers in $[Cu(hfac)_2(TTF\text{-}py)_2](PF_6)\cdot 2CH_2Cl_2$[12] [hfac = hexafluoroacetylacetonate and TTF-py = 4-(2-tetrathiafulvalenylethenyl)pyridine], by connecting TTF to the Cu^{II} complex by unsaturated bonds and rings. So far, however, this approach has led to molecular compounds with very poor conducting properties and lack of magnetic properties of interest.

Some of us have also been interested in combining conductivity and magnetism by using metallocenium and $M(dmit)_2$ complexes.[13] Despite the interesting magnetic properties observed in $(Cp^*_2Mn)[Ni(dmit)_2]$, no fractional oxidation-state compound has been obtained with metallocenium and, consequently, the compound is an insulator. Another way of introducing a magnetic component into $M(dmit)_2$ complexes is to use spin-crossover cations. Spin crossover (abbreviated as SCO) in certain transition metal complexes has been known for a long time and has been well described and studied by several authors.[14] From the perspective of the present work, it should be noted that a slight modification in the ligand or in the nature of the solvent might result in a change of the value of the transition temperature, or even in the vanishing of the SCO phenomenon.

The ultimate goal of this work is to obtain a molecular conductor, and consequently a complex in a fractional oxidation state, that exhibits a spin crossover in such a way that the bistability of this magnetic switch may affect the conducting properties of the material. The choice of the starting SCO complex is crucial in the sense that it must not lose its magnetic properties when combined with the $M(dmit)_2$ complex. It must also not decompose or undergo any transformation during the oxidation process necessary to obtain the fractional oxidation state of the complex. In this context, Fe^{III} complexes seem promising as their oxidation state should not change during the synthesis of the fractional oxidation-state complex.

Several Fe^{III} complexes displaying SCO have already been described (see ref.[15] for a comprehensive review). In six-coordinate Fe^{III} systems an $S = 1/2 \leftrightharpoons S = 5/2$ conversion was observed in most cases. In these Fe^{III} SCO complexes, similar to the "benchmark" Fe^{II} complexes, the LS to HS spin-state change is accompanied by an increase of the metal–ligand distances ($\Delta r \approx 8$–15%). However, the average bond length change is significantly smaller in the case of Fe^{III} ions ($\Delta r \approx 5\%$) than for Fe^{II}. Due to this fact, the rate of interconversion of spin states is, in general, faster in Fe^{III} systems to such an extent that in many instances the ^{57}Fe Mössbauer spectra do not show separate HS and LS contributions. It is mainly for this reason that, in contrast to Fe^{II} compounds, a light-induced spin-state trapping (LIESST) effect is rarely observed in Fe^{III} complexes.[16–18] Furthermore, the majority of Fe^{III} SCO complexes display a gradual spin-state change as a function of temperature, while abrupt transitions with thermal hysteresis have been reported in only a few cases.[19–25] Although in a less straightforward way, this tendency may also be related to the smaller bond length changes in Fe^{III} complexes, given that the lattice expansion is a major ingredient for the cooperative interactions (elastic interactions) determining the gradual/abrupt nature of the spin-transition curves.[26]

For another attempt to obtain SCO properties in a molecular conductor (see ref.[19] for the first attempt), we chose the SCO complex [Fe(salten)Mepepy](BPh_4), previously reported by Sour et al.[27] [H_2salten = 4-azaheptamethylene-1,7-bis(salicylideneiminate); Mepepy = 1-(pyridin-4-yl)-2-(*N*-methylpyrrol-2-yl) ethane]. This Fe^{III} complex exhibits a gradual, thermally induced SCO.[27] Moreover, it also undergoes a partial photoinduced spin-state change in solution due to the photoisomerizable ligand Mepepy. Such a physical property might also play a role in the electrical properties of the final compound.

In this paper, we report the synthesis and X-ray characterisation of three new iron(III) compounds of formula [Fe(salten)Mepepy][$Ni(dmit)_2$] and [Fe(salten)Mepepy]-[$M(dmit)_2$]·CH_3CN (M = Pd, Pt), together with magnetic, spectroscopic and Mössbauer studies of the Ni derivative.

Results and Discussion

Description of the Structures

To the best of our knowledge this is the first time that the structure of complexes containing the Fe(salten)-(Mepepy) unit has been reported. The triclinic unit cell of each compound contains one $M(dmit)_2$ unit and one Fe(salten)(Mepepy) unit, with one acetonitrile molecule for the Pd and Pt complexes only (Figure 1).[28] Selected crystallographic data for every compound are reported in the Experimental Section (general crystallographic data can be found in the Supporting Information, Table S1).

Considering the cell parameters, the cell volume decreases upon lowering the temperature for every compound (see Table 1). For the Pd and Pt complexes, this decrease is accompanied by a decrease of the value for all parameters except the angles β and γ, whose values increase slightly. The Ni complex exhibits other features: only the β value increases when lowering the temperature, although the b and a values first decrease (from 295 to 240 K), and then increase again down to 100 K.

The intramolecular distances and angles within the $M(dmit)_2$ units are similar to those observed in other monoanionic $M(dmit)_2$ complexes.[29] In every complex, the Fe atom is in an octahedral environment, with the two oxygen atoms in a *trans* configuration. The two largest bond lengths around Fe are Fe–N21 and Fe–N32; the two shortest are Fe–O11 and Fe–O12. Thus, the [FeO_2N_4] octahedron can be regarded as axially elongated along the N32–Fe–N21 direction or axially compressed along the O11–Fe–O12 direction. The Mepepy fragment is not planar due to a slight distortion around the central C=C ethene bond:

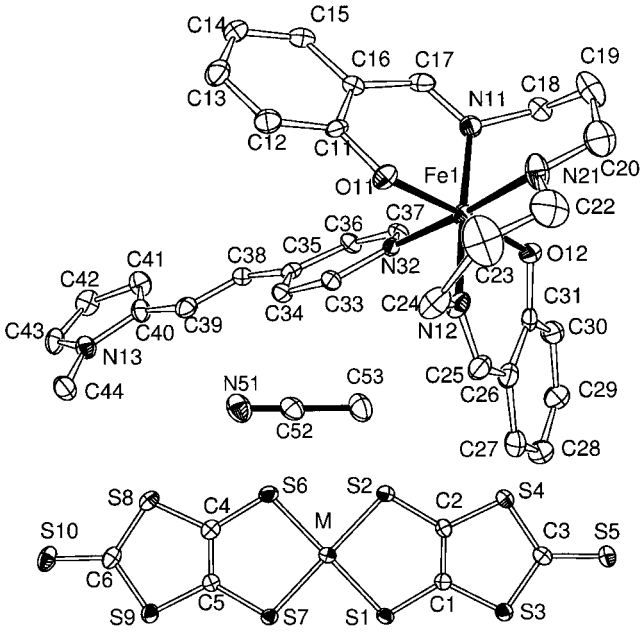

Figure 1. Asymmetric unit showing the atomic labelling of [Fe(salten)Mepepy][M(dmit)$_2$] (M = Ni, Pd, Pt) with acetonitrile present for M = Pd and Pt.

Table 1. Variations of the cell parameters (%, vs. parameters at 295 K) for **1**, **2** and **3** at 240, 160 and 100 K.

	T	Δ*a*/*a*	Δ*b*/*b*	Δ*c*/*c*	Δ*a*/*a*	Δ*β*/*β*	Δ*γ*/*γ*	Δ*V*/*V*
	240	–0.4	–0.2	–1.2	–0.2	0.2	–0.4	–1.7
Ni	160	–0.9	–0.1	–1.8	–0.2	0.2	–0.4	–2.8
	100	–1.1	–0.1	–1.9	–0.1	0.4	–0.4	–3.3
	240	–0.3	0.0	–0.5	–0.1	0.1	0.1	–0.9
Pd	160	–0.7	–0.3	–1.0	–0.2	0.2	0.1	–2.3
	100	–0.9	–0.4	–1.3	–0.3	0.3	0.2	–3.0
	240	–0.6	–0.2	–0.8	–0.2	0.1	0.0	–1.7
Pt	160	–1.0	–0.5	–1.3	–0.2	0.2	0.1	–2.9
	100	–1.2	–0.6	–1.7	–0.4	0.3	0.2	–3.7

the dihedral angle of C35–C38–C39–C40 ranges between 173.62(45)° (Ni, 100 K) and –179.90(41)° (Pd, 160 K; see Figure 2 and Table 2).

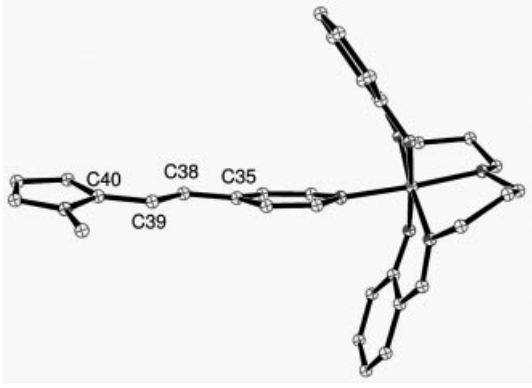

Figure 2. View of the [Fe(salten)Mepepy]$^+$ cation showing the non-planarity of the Mepepy part.

Table 2. Dihedral angle around C35–C38–C39–C40 and angle between the pyridine ring and the methylpyrrole ring in **1**, **2** and **3** at various temperatures.

		295 K	240 K	160 K	100 K
Dihedral angle around	Ni	176.0(8)	176.1(6)	175.9(6)	173.6(5)
C35–C38–C39–C40	Pd	179.6(5)	179.7(4)	–179.9(4)	–179.4(4)
	Pt	178.8(6)	178.6(8)	179.1(6)	179.6(53)
Angle between the pyridine ring	Ni	10.7(7)	11.0(5)	12.0(5)	11.4(4)
and the methylpyrrole ring	Pd	14.0(4)	14.3(4)	14.3(4)	14.5(3)
	Pt	12.7(5)	12.9(6)	13.0(5)	13.4(4)

Three different temperature effects are observed for each complex: for the Ni complex, lowering the temperature induces a decrease of this torsion angle [from 176.0(8)° to 173.6(5)°], whereas it increases in the Pt complex [from 178.8(6)° to 179.6(5)°]. For the Pd complex, a rocking motion is observed from 179.6(5)° to –179.4(4)°. These variations in the dihedral angle around the central C=C bond also induce a non-planarity between the two rings of the Mepepy fragment. The angle between the pyridine ring and the methylpyrrole ring ranges between 10.7(7)° (Ni, 295 K) and 14.5(3)° (Pd, 100 K; see Table 2). Whatever the complex, this angle always increases when the temperature is lowered. In regard to the latter two parameters (dihedral angle and inter-planar angle), the largest deviations are observed for the Ni complex.

The bond lengths around Fe also decrease when lowering the temperature (see Table 3). The bonds Fe–N32 and Fe–N11 are the most sensitive to the temperature: they exhibit variations up to around –3.2% between 295 K and 100 K (for the Pt complex, bond Fe–N32). For every complex, a decrease of the temperature tends to reduce the gap between the different bond lengths: indeed, since the longest bond lengths are subject to the largest decrease, this induces a more regular distribution of the bond lengths around the Fe atom.

Depending on the temperature, the twelve angles subtended at the Fe atom do not vary similarly as some decrease whereas others increase. A noticeable point is the following: whatever the complex, the O11–Fe–N12 and N12–Fe–N32 angles decrease down to around –2.5% and the O11–Fe–N11 angle increases by up to about 2.0% when compared to their value at room temperature. The Pd complex is the one for which there are the smallest variations in the values of distances and angles around the Fe atom.

Deformations of the octahedron around Fe can be estimated from the angles between the three equatorial planes defined by the six Fe-coordinating atoms, together with the deviation of the central Fe atom from these planes. These planes are almost orthogonal to each other, as reflected by the values all larger than 88° (Table S2 in the Supporting Information), and the Fe atom always lies very close to these planes (max. deviation of 0.024 Å). The angles between the eight opposite faces of the octahedron around Fe also define its deformation: at room temperature, these values lie between 3.99° and 6.31°, thus indicating that the faces are not parallel (Table S2 in the Supporting Infor-

Table 3. Bond lengths around the Fe atom with their variations [%] relative to the room temperature values for **1**, **2** and **3** at various temperatures.

		Ni		Pd		Pt	
		Bond length	Δ%	Bond length	Δ%	Bond length	Δ%
Fe(1)–O(11)	295	1.926(5)	0.0	1.884(4)	0.00	1.892(5)	0.00
	240	1.890(4)	–1.8	1.877(3)	–0.37	1.900(5)	0.42
	160	1.885(4)	–2.1	1.872(3)	–0.64	1.887(4)	–0.32
	100	1.891(3)	–1.8	1.872(3)	–0.64	1.880(4)	–0.63
Fe(1)–O(12)	295	1.884(6)	0.0	1.899(4)	0.00	1.901(5)	0.00
	240	1.868(4)	–0.8	1.889(3)	–0.53	1.906(5)	0.26
	160	1.871(4)	–0.7	1.887(3)	–0.63	1.874(5)	–1.42
	100	1.873(3)	–0.6	1.884(3)	–0.79	1.877(4)	–1.26
Fe(1)–N(11)	295	1.979(9)	0.0	1.965(4)	0.00	1.971(5)	0.00
	240	1.949(5)	–1.5	1.953(3)	–0.61	1.959(7)	–0.61
	160	1.916(6)	–3.2	1.946(3)	–0.97	1.947(5)	–1.27
	100	1.930(4)	–2.5	1.947(3)	–0.92	1.930(5)	–2.08
Fe(1)–N(12)	295	1.979(8)	0.0	1.972(4)	0.00	1.987(6)	0.00
	240	1.925(5)	–2.7	1.961(4)	–0.56	1.990(7)	0.15
	160	1.937(5)	–2.1	1.958(3)	–0.71	1.971(5)	–0.86
	100	1.935(4)	–2.2	1.959(3)	–0.66	1.957(5)	–1.51
Fe(1)–N(21)	295	2.057(10)	0.0	2.033(5)	0.00	2.044(7)	0.00
	240	2.033(5)	–1.2	2.016(4)	–0.84	2.003(8)	–2.01
	160	1.994(6)	–3.1	2.018(4)	–0.74	1.999(6)	–2.05
	100	2.013(4)	–2.1	2.019(4)	–0.69	2.009(5)	–1.71
Fe(1)–N(32)	295	2.049(7)	0.0	2.036(4)	0.00	2.052(5)	0.00
	240	2.023(4)	–1.3	2.006(3)	–1.47	2.019(6)	–1.61
	160	1.983(6)	–3.2	1.994(3)	–2.06	2.001(5)	–2.53
	100	1.993(4)	–2.7	1.994(3)	–2.06	1.986(5)	–3.22

mation). In most cases a decrease of the temperature tends to reduce these angles (up to –3.23° for the Ni complex). These features, together with those discussed above, clearly show that the distorted octahedral environment around Fe tends to become more and more regular as well as more compact upon decreasing the temperature.

The structure can also be viewed as layers of iron complexes together with acetonitrile, separated from each other by layers of $M(dmit)_2$ units (Figure 3).

Each layer spreads out almost in the $(01\bar{1})$ plane. There are several short intermolecular contacts (around the sum of the van der Waals radii) within each layer. Within the $M(dmit)_2$ layers, short intermolecular contacts below 3.7 Å involve parallel $M(dmit)_2$ units connected through S–S interactions (Figure 3). Depending on M and the temperature, the units are connected through 1, 3, 5 or 7 contacts (≤3.7 Å) between S atoms. For a given M, the lower the temperature the larger the number of contacts (see Supporting Information, Table S3).

In addition, there are also some short intermolecular contacts (interatomic distances ≤ sum of the van der Waals radii[30]) between the sheets of $M(dmit)_2$ units and the layer of iron complexes and solvent (see Supporting Information, Table S4).

There is no contact between the acetonitrile and $M(dmit)_2$ units, whatever M is. Acetonitrile, if present, is connected through short contacts (see Supporting Information, Table S5) to the Fe units only.

The iron complexes are also connected to each other through several short contacts (see Supporting Information, Table S6), but no real hydrogen bonds exist. As for the interactions between the $M(dmit)_2$ units, the lower the temperature the larger the number of contacts between the various components of these compounds.

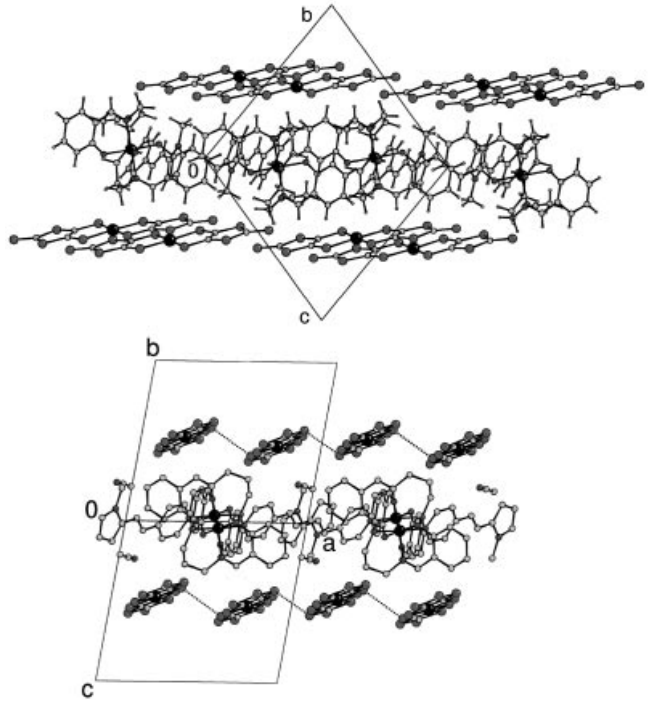

Figure 3. View of the structural arrangement in **1**, **2** and **3** along the *a* direction (left) and along the *bc* direction (right).

UV/Vis Spectroscopy and Light Irradiation Effects

The UV/Vis absorption spectrum of [Fe(salten)Mepepy](BPh$_4$) in CH_2Cl_2 is shown in Figure 4. It shows two strong and broad absorption bands (λ = 370 nm, ε = 17757 $M^{-1}cm^{-1}$; λ = 401 nm, ε = 16656 $M^{-1}cm^{-1}$) and a very weak band (λ = 486 nm, ε = 4803 $M^{-1}cm^{-1}$). This latter is due to a ligand-to-metal charge transfer (LMCT).[27] Whereas only one band (λ = 375 nm) is observed in CH_3CN,[27] the splitting and broadening of this transition in CH_2Cl_2 is probably due to solvent effects (smaller polarity of CH_2Cl_2 compared with CH_3CN), which change the energy of the electronic transitions and induce bathochromic and hypsochromic shifts. Nevertheless, the transitions at 370 and 401 nm can be assigned to a ligand-centred $\pi\rightarrow\pi^*$ transition similar to that observed in CH_3CN.[27] Upon irradiation, these transitions are slightly blue-shifted (from 371 to 364 nm, and from 401 to 397 nm), and their intensities are significantly decreased (from 17757 to 11667 $M^{-1}cm^{-1}$, and from 16656 to 11109 $M^{-1}cm^{-1}$). As in CH_3CN, the LMCT transition at 486 nm is not affected by light.[27] From this study on the starting [Fe(salten)Mepepy](BPh$_4$) salt, it can be concluded that this complex also undergoes a *trans* to *cis* isomerisation of the Mepepy ligand in CH_2Cl_2.

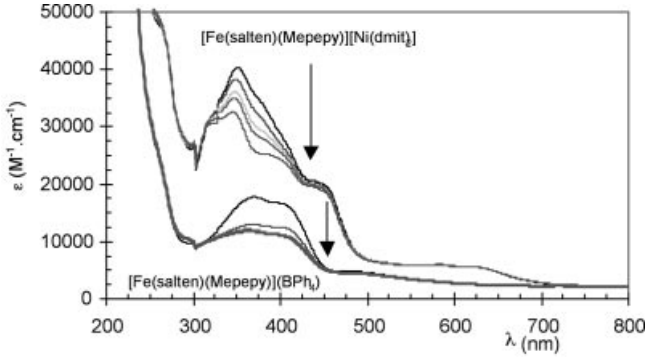

Figure 4. UV/Vis spectra and evolution upon irradiation of [Fe(salten)Mepepy](BPh$_4$) (lower curves) and [Fe(salten)Mepepy][Ni(dmit)$_2$ (upper curves) in CH_2Cl_2. Arrows indicate decrease of the intensity of the transitions upon irradiation.

The effect of light was then studied for the [Fe(salten)Mepepy][Ni(dmit)$_2$] complex in solution. The UV/Vis spectrum of this complex exhibits several absorption peaks. The main absorption band lies around 351 nm (ε = 40288 $M^{-1}cm^{-1}$) and contains several shoulders at shorter and longer wavelengths. This broad peak is the superposition of several transitions within the $[Ni(dmit)_2]^-$ unit ($\pi\rightarrow\pi^*$ and MLCT transitions[31]) and includes the transitions previously observed in the starting salt [Fe(salten)Mepepy](BPh$_4$). A satellite band is observed at 443 nm ($\pi\rightarrow\pi^*$, $\varepsilon \approx$ 20412 $M^{-1}cm^{-1}$) and two weaker bands at 582 nm ($n_S\rightarrow\pi^*$[31]) and 620 nm (with $\varepsilon \approx$ 6000 and 5600 $M^{-1}cm^{-1}$, respectively), attributed to MLCT transitions.[32] Irradiation results in a blue shift of the most important absorption (from 351 to 345 nm), accompanied by a decrease of ε = 32407 $M^{-1}cm^{-1}$. The shoulders also become more pronounced, and one is clearly visible at 385 nm (ε = 24992 $M^{-1}cm^{-1}$). The bands at 443, 582 and 620 nm are unaffected by irradiation. The absorption at 385 nm can be attributed to the ligand-centred $\pi\rightarrow\pi^*$ transition {initially at 370 nm in the starting salt [Fe(salten)Mepepy](BPh$_4$)}. Upon irradiation, this transition exhibits a decrease of around 25% of its intensity. The parallel evolution of the starting salt [Fe(salten)Mepepy](BPh$_4$) and [Fe(salten)Mepepy][Ni(dmit)$_2$] suggests that the $[Fe(salten)Mepepy]^+$ unit also undergoes an isomerisation in solution when associated with the $[Ni(dmit)_2]^-$ unit.

Raman Studies of the [Fe(salten)Mepepy]-Based Complexes

It is possible to evaluate the charge transfer in complexes containing $[Ni(dmit)_2]^{n-}$ units (in an entire or fractional oxidation state) by Raman spectroscopy.[33] The Raman spectrum of [Fe(salten)Mepepy][Ni(dmit)$_2$] is shown in Figure 5a. The lines at 599, 1435 and 1598 cm^{-1} were assigned to the Fe(salten) fragment in comparison with the spectra of [Fe(salten)]Cl (see Figure S2, Supporting Information). The lines at 134, 338, 357, 508, 1051 and 1395 cm^{-1} were assigned to the $[Ni(dmit)_2]^-$ unit by comparison with literature data,[33] and confirm that the charge transfer, ρ, is equal

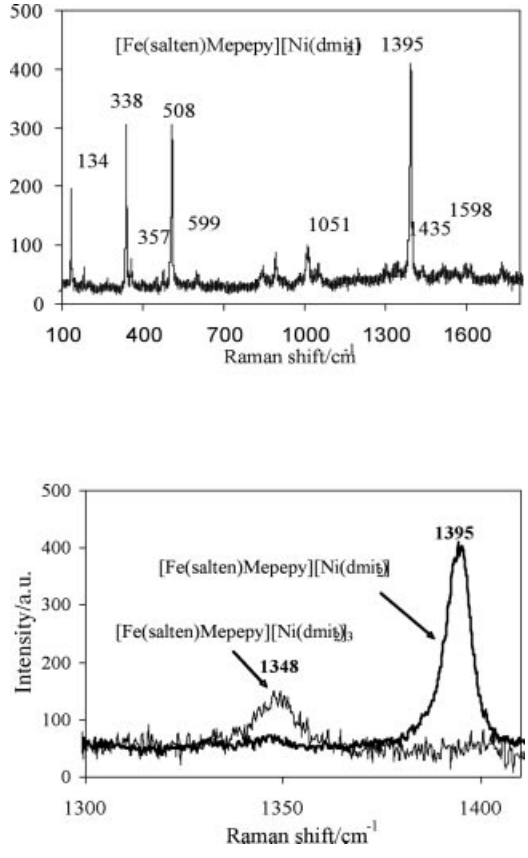

Figure 5. Raman spectra of a single crystal of [Fe(salten)Mepepy][Ni(dmit)$_2$] (top) and [Fe(salten)Mepepy][Ni(dmit)$_2$]$_3$ (bottom).

to 1. In [Fe(salten)Mepepy][Ni(dmit)$_2$] the band at 1395 cm^{-1} is due to the C=C bond stretching mode. In [Fe(salten)Mepepy][Ni(dmit)$_2$]$_x$, this line (Figure 5b) is found at 1348 cm^{-1}. This band, whose position is very sensitive to the amount of charge transfer, allows us to determine a ρ value of around 0.3. The others lines of this spectrum are due to the Ni(dmit)$_2$ fragment and are in agreement with this ratio (Table S7, Supporting Information).

Magnetic Properties of Non-Fractional Oxidation State Complexes

For the Ni and Pt complexes (Figure 6), the temperature dependence of the $\chi_M T$ product shows a rapid but gradual decrease down to about 235 K, followed by a slightly descending plateau down to 2 K, with a slope about 10 times smaller than in the previous region and with a $\chi_M T$ product close to 0.9 cm^3 K mol^{-1} (χ_M = molar magnetic susceptibility).

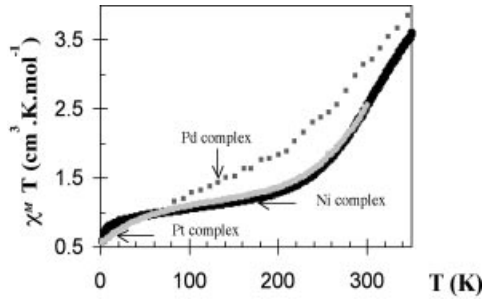

Figure 6. Variations of $\chi_M T$ as a function of the temperature for **1**, **2** and **3**.

For the Ni complex the magnetic properties are the same with or without acetonitrile in the complex (see Supporting Information, Figure S1). The Pd complex, which has been measured only between 80 and 350 K, exhibits almost similar behaviour, but with a smaller change in the slope at around 210 K. No plateau is observed down to 80 K. The behaviours of the Ni and Pt complexes are very close and similar to that observed for the starting iron salt [Fe(salten)-Mepepy](BPh$_4$).[27] For a given complex, the magnetic behaviour in the warming and cooling modes does not show any detectable thermal hysteresis loop. The 1:1 stoichiometry of the complexes [Fe(salten)Mepepy][M(dmit)$_2$] (M = Ni, Pd, Pt)} shows they are built on the association of an Fe^{III} complex with a formally M^{III} complex with S = 1/2.

Neglecting any magnetic interaction between Fe^{III} and M^{III}, as well as the orbital contributions, the expected "spin-only" value of $\chi_M T$ is equal to 4.38 cm^3 K mol^{-1} for Fe^{III} ions in the high-spin (HS) state (S = 5/2) and 0.37 cm^3 K mol^{-1} for both the M^{III} ions and the Fe^{III} ions in the low-spin (LS) state (S = 1/2). At the highest temperatures of the measurements, the experimental values are about 3.5 cm^3 K mol^{-1}, which are clearly below the expected values (ca. 4.8 cm^3 K mol^{-1}). In the low-temperature regime the experimental plateau is above the expected value (ca. 1.0 cm^3 K mol^{-1} compared to 0.74 cm^3 K mol^{-1}). These observations indicate that the spin transition is incomplete both at low and at high temperatures, i.e. at 350 K a fraction of Fe^{III} ions is still in the LS form, while there is a residual HS fraction even at the lowest temperatures, as confirmed by the Mössbauer data (see below).

Fitting the temperature dependence of the HS fraction (curve not shown) with the well-known Ising-like model[34–36] leads to the thermodynamic parameters of the spin crossover in this compound: an energy gap between the HS and LS levels, Δ, of 1536 cm^{-1} and a reasonable entropy change upon the spin crossover of ΔS = 33 J K^{-1} mol^{-1}. The fitting also leads to a very weak cooperative interaction ($J \approx 0$ cm^{-1}), in accordance with a non-cooperative system.

In summary, these results clearly show that the spin conversion is maintained in the Fe complex, even after the substitution of the BPh$_4^-$ anion by the [M(dmit)$_2$]$^-$ anion. This latter seems, therefore, to have a "neutral" effect on the magnetic properties of the [Fe(salten)Mepepy]$^+$ complex, whereas it has a "positive" effect when combined with [Fe(sal$_2$trien)]$^+$ (appearance of a strong cooperativity and a hysteresis loop, never observed before in this family of SCO complexes).[19]

Magnetic Properties of the Fractional Oxidation State Complex

A plot of the $\chi_M T$ product vs. temperature is shown in Figure S3 (Supporting Information). $\chi_M T$ is equal to 1.47 cm^3 K mol^{-1} at room temperature, and decreases almost linearly down to a value of 0.04 cm^3 K mol^{-1} at 2 K. Such a behaviour can be explained by a gradual spin conversion of the [Fe(salten)Mepepy]$^+$ unit from the HS state to the LS state, coupled to an antiferromagnetic interaction between the two components, which leads at low temperature to a non-magnetic ground spin state. This explanation is in agreement with a lack of magnetisation at 2 K (see Figure S4 in the Supporting Information).

Mössbauer studies were not possible in the present case because of the small amount of sample available (0.8 mg). For the same reason, room temperature electrical conductivity was only measured on the powder by the two-probes method. A value as large as 0.1 S cm^{-1} was obtained, which is indicative of the presence of a significant electron delocalisation in this compound.

Mössbauer Spectroscopy

The ^{57}Fe Mössbauer spectra of [Fe(salten)Mepepy]-[Ni(dmit)$_2$] were recorded between 4.5 K and 330 K. Figure 7 show selected spectra obtained in the cooling mode. The fitted Mössbauer parameters at each temperature are given in Table 4.

Table 4. Least-squares-fitted Mössbauer data for [Fe(salten)Mepepy][Ni(dmit)$_2$].

	Low spin[a,b]			High spin			
T [K]	δ [mm s^{-1}]	ΔE_Q [mm s^{-1}]	$\Gamma/2$ [mm s^{-1}]	δ [mm s^{-1}]	ΔE_Q [mm s^{-1}]	$\Gamma/2$ [mm s^{-1}]	A_{HS}/A_{tot}
4.5	0.23(1)	1.74(1)	0.31(1)	0.41(5)	–0.6(1)	0.51(8)	19(2)
80	0.254(2)	1.649(4)	0.277(3)	0.466(8)	0.68(1)	0.277(3)	24(1)
150	0.242(3)	1.528(6)	0.266(5)	0.446(5)	0.64(2)	0.266(5)	31(1)
185	0.227(3)	1.451(8)	0.233(6)	0.426(6)	0.65(1)	0.233(6)	34(1)
220	0.225(3)	1.392(7)	0.223(6)	0.413(5)	0.646(9)	0.223(6)	39(1)
260	0.22(2)	1.14(3)	0.24(1)	0.39(2)	0.67(3)	0.24(1)	50(3)
300	0.14(3)	1.05(8)	0.24(5)	0.34(1)	0.658(2)	0.24(1)	80(4)
330	0.2(1)	0.8(2)	0.27(1)	0.349(5)	0.62(1)	0.27(1)	78(5)

[a] δ = isomer shift; ΔE_Q = quadrupole splitting; $\Gamma/2$ = half-height width of the line; A_{HS}/A_{tot} = area ratio. [b] Error bars are given in parentheses; isomer-shift values refer to metallic iron at room temperature. Between 80 and 330 K both components were fitted with the same linewidth.

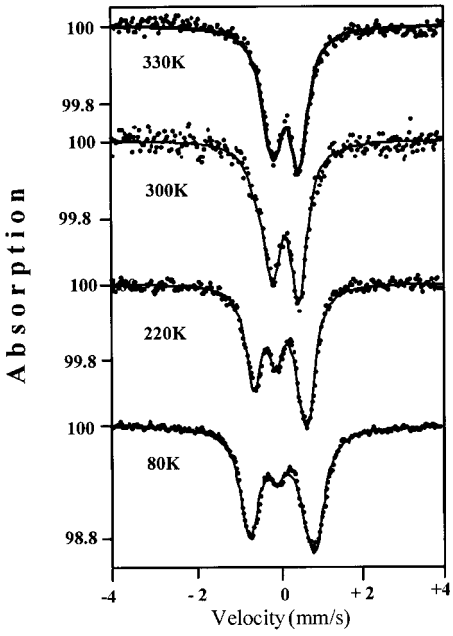

Figure 7. Selected Mössbauer spectra of [Fe(salten)Mepepy][Ni(dmit)$_2$] obtained in the cooling mode between 330 and 80 K. The solid lines represent fitted curves.

At 330 K, the spectrum for [Fe(salten)Mepepy][Ni(dmit)$_2$] consists chiefly (80%) of one component with isomer-shift and quadrupole-splitting values characteristic of HS Fe^{III}. The ratio of the LS component increases gradually with decreasing temperature. This component is characterised by somewhat larger isomer-shift and quadrupole-splitting values. It is important to note that, in contrast to the first doublet, this second spectrum exhibits almost no temperature dependence of the quadrupole splitting. Taking into account that in the ^{6}S configuration of Fe^{III} no low-lying excited levels are expected and its $^2T_{2g}$ configuration shows an appreciable thermal population of close-lying excited levels when slightly distorted, the low-temperature main doublet (76%) can be assigned unambiguously to a low-spin Fe^{III} species and the high-temperature main doublet (78%) corresponds to a high-spin Fe^{III} species. The distinct spectra obtained for the two spin-states indicate that the spin interconversion rates are slow compared to the hyperfine frequencies of Mössbauer spectroscopy (ca. 10^{-7}–10^{-8} s^{-1}]). The area ratio A_{HS}/A_{tot}, which is in a first approximation proportional to the HS fraction, decreases gradually from 330 K (≈78%) to 80 K (≈24%). It must be emphasised that the Mössbauer data were collected for the same sample that was studied with magnetic susceptibility. In spite of this, the HS fraction that can be deduced from the Mössbauer spectra (Table 4) and magnetic susceptibility data (Figures 6 and 7) are slightly different, especially in the high-temperature region (300 and 330 K). Among the reasons for this discrepancy one should note that the magnetic data are difficult to convert into HS fractions since the susceptibilities of the pure HS and LS species are not known. Furthermore, the high-temperature Mössbauer spectra are not sufficiently resolved (due to the close isomer-shift and quadrupole-splitting values of Fe^{III} in both states) and therefore there is a large uncertainty in the fits. On the whole, however, the Mössbauer data clearly confirm the gradual and incomplete $S = 1/2 \leftrightharpoons S = 5/2$ spin crossover of Fe^{III} species in [Fe(salten)Mepepy][Ni(dmit)$_2$].

Upon further cooling to 4.5 K a magnetic hyperfine splitting appears. The spectrum (Figure 8) shows that only the quadrupolar doublet corresponding to the residual HS fraction is converted into a magnetic hyperfine Mössbauer splitting.

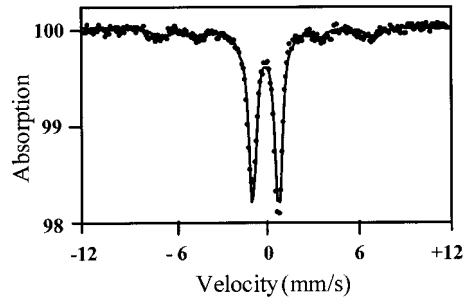

Figure 8. Mössbauer spectrum of [Fe(salten)Mepepy][Ni(dmit)$_2$] at 4.5 K. The solid line represents the fitted curve with both quadrupolar and magnetic components.

The spectrum was fitted by an axial hyperfine magnetic field parallel to the principal axis of the electric field gradient (EFG). The fit shows unambiguously that the principal EFG component is negative. In addition, the corresponding

hyperfine magnetic field, H_i, was evaluated to be 430 kOe. This value falls in the range expected for HS Fe^{III}.[37] The magnetic component of the spectrum was fitted with quite a large line-width [$\Gamma/2 = 0.51(8)$ mm s^{-1}], thus indicating the presence of some magnetic relaxation in the system. It should be noted, however, that the H_i value obtained here (430 kOe) is somewhat smaller than what can be expected from the $220<S_z>$ rule, which leads to a theoretical value of $H_i = 550$ kOe. This is due to the fact that the magnetic ordering at 4.5 K is not totally achieved and needs a lower temperature to be complete, in good agreement with the observation of the broadening of the linewidth at this temperature. One can attribute this magnetic splitting at 5 K either to a slow paramagnetic relaxation or to a long-range cooperative order. Considering the first possibility (slow paramagnetic relaxation), the dilute nature of the complex is evidenced by a shortest inter-complex Fe^{III}–Fe^{III} distance of about 6.9 Å, a magnitude which is large enough to result in long spin-spin relaxation times for high-spin iron(III). Considering the possibility of a long-range order, on the basis of the magnetic data we cannot exclude the possibility of the existence of magnetic couplings, even though it seems more reasonable to describe the low-temperature variation of magnetic properties in terms of zero-field splitting effects. We note that these limiting behaviours can be distinguished by Mössbauer spectroscopy by analysis of the temperature dependence of the spectra using the Mössbauer magnetic relaxation theory established by Blume and Tijon.[38] It can be also achieved experimentally using a weak external applied magnetic field, which may freeze the magnetic fluctuations.[39] These laborious approaches, however, are beyond the scope of this paper.

Conclusions

In attempt to combine conductivity and spin-crossover properties in the same material, we have synthesised three new compounds with the general formula [Fe(salten)Mepepy][M(dmit)$_2$]·CH_3CN (M = Ni, Pd, Pt). We have shown by magnetic susceptibility and Mössbauer measurements that the Fe^{III} ions preserve their spin-crossover properties in the new crystal lattice, although the spin crossover of the Ni complex is not complete at low temperature (80 K). Mössbauer spectroscopy has shown that the remaining high-spin state is magnetically ordered at 4.5 K, leading to a promising way to combine magnetic properties and bistability in inorganic molecular compounds. Preliminary attempts to synthesise fractional oxidation-state complexes have resulted in the synthesis of a conductive powder that exhibits a spin conversion with antiferromagnetic interactions. Although not structurally characterised, this compound is one of the first complexes to combine spin conversion and electrical properties. Work is currently in progress to combine such SCO compounds with metal-bisdithiolene complexes.[19]

Experimental Section

Synthesis: All reactions were performed under an inert atmosphere of argon, using Schlenk technique, and sheltered from daylight. Solvents were dried and distilled under argon prior to use.

[Fe(salten)Mepepy](BPh$_4$) and (NBu$_4$)[M(dmit)$_2$] (M = Ni, Pd, Pt) were synthesised following literature methods.[27,40]

Synthesis of [Fe(salten)Mepepy][M(dmit)$_2$]·CH_3CN (M = Ni, Pd, Pt): (NBu$_4$)[M(dmit)$_2$] (M = Ni, Pd, Pt; 0.24 mmol) was dissolved in a mixture of acetonitrile and acetone (30 and 20 mL, respectively) and a solution of [Fe(salten)Mepepy](BPh$_4$) (214 mg, 0.24 mmol) in acetonitrile (10 mL) was added dropwise. The resulting solution was stirred for 5 min and stored at 4 °C overnight. The precipitate obtained was filtered, washed with 5 × 5 mL of acetonitrile, 2 × 3 mL of diethyl ether, and dried under vacuum. Every compound was obtained as shiny, crystalline blocks, which were used for subsequent characterisations. Initially, the Ni complex was obtained with acetonitrile (its structure was solved at 160 K, see below). The same crystal, when analysed again a few weeks later on the diffractometer, did not contain acetonitrile.

1: [Fe(salten)Mepepy][Ni(dmit)$_2$]. $C_{38}H_{35}FeN_5NiO_2S_{10}$ (1028.9): calcd. C 44.36, H 3.43, N 6.81; found C 44.95, H 3.53, N 6.89.

2: [Fe(salten)Mepepy][Pd(dmit)$_2$]·CH_3CN. $C_{40}H_{38}FeN_6O_2PdS_{10}$ (1117.6): calcd. C 42.98, H 3.43, N 7.52; found C 42.95, H 3.58, N 7.10.

3: [Fe(salten)Mepepy][Pt(dmit)$_2$]·CH_3CN. $C_{40}H_{38}FeN_6O_2PtS_{10}$ (1206.3): calcd. C 39.82, H 3.18, N 6.97; found C 40.50, H 3.04, N 6.46.

Synthesis of [Fe(salten)Mepepy][Ni(dmit)$_2$]$_3$: This complex was obtained either by galvanostatic or potentiostatic oxidation of [Fe(salten)Mepepy][Ni(dmit)$_2$] in acetonitrile, using Pt electrodes.

UV/Vis Spectroscopy/Irradiation: Measurements were performed with [Fe(salten)Mepepy](BPh$_4$) and [Fe(salten)Mepepy][Ni(dmit)$_2$] at room temperature in CH_2Cl_2 solution with a Perkin–Elmer Lambda 5 equipment. Irradiation was performed with a 200 W (Hg) Oriel lamp (filter 400 nm).

X-ray Structure Analysis: X-ray data for each compound, were collected at 295, 240, 160 and 100 K on an IPDS diffractometer (Stoe) or on an Xcalibur (Oxford Diffraction) diffractometer, with monochromatic Mo-K_α radiation ($\lambda = 0.71073$ Å). Crystallographic data are given in Table 5. X-ray structure analysis was performed using the WinGX package.[41] H atoms were included at their calculated positions as riding on their adjacent atom. SIR97[42] or Shelxs97[43] were used for the structure solutions, Shelxl97[44] for the refinements, Platon[45] for structure analysis, and Ortep3[46] or Cameron[47] for the production of the crystallographic illustrations. CCDC-262730 to -262742 contain the supplementary crystallographic data for this paper. These data can be obtained free of charge from The Cambridge Crystallographic Data Centre via www.ccdc.cam.ac.uk/data_request/cif.

Magnetic Measurements: Magnetic measurements were performed on powders (Pd and Pt complexes containing acetonitrile; Ni complex without acetonitrile) using either an MPMS SQUID magnetometer (Quantum Design) operating at 1 T or a Faraday-type magnetometer equipped with a DRUSH electromagnet (operating in the range 0.4–1.4 T), a Sartorius balance and a continuous-flow Oxford Instruments cryostat. The magnetic susceptibility values were calibrated against Hg[Co(SCN)$_4$]. Data were corrected for magnetisation of the sample holder and for diamagnetic contributions, which were estimated from Pascal's constants.

Table 5. Crystallographic data for the complexes [Fe(salten)Mepepy][M(dmit)$_2$] at various temperatures.

	[Fe(salten)Mepepy][Ni(dmit)$_2$] (**1**)				[Fe(salten)Mepepy][Pd(dmit)$_2$]·CH$_3$CN (**2**)				[Fe(salten)Mepepy][Pt(dmit)$_2$]·CH$_3$CN (**3**)			
Empirical formula	$C_{38}H_{35}FeN_5NiO_2S_{10}$				$C_{40}H_{38}FeN_6O_2PdS_{10}$				$C_{40}H_{38}FeN_6O_2PtS_{10}$			
M	1028.87				1117.61				1206.30			
Temperature [K]	293	240	160	100	280	240	160	100	293	240	160	100
Crystal system	triclinic				triclinic				triclinic			
Space group	$P\bar{1}$				$P\bar{1}$				$P\bar{1}$			
Z	2				2				2			
a [Å]	13.384(2)	13.335(3)	13.262(3)	13.239(1)	13.433(2)	13.394(1)	13.333(5)	13.306(1)	13.464(2)	13.384(1)	13.332(2)	13.303(3)
b [Å]	12.995(2)	12.971(3)	12.983(3)	12.987(1)	13.541(2)	13.536(2)	13.503(5)	13.483(2)	13.556(1)	13.522(2)	13.485(2)	13.469(3)
c [Å]	14.972(2)	14.785(3)	14.699(3)	14.684(1)	14.811(2)	14.740(2)	14.658(5)	14.613(2)	14.832(2)	14.712(1)	14.635(2)	14.587(3)
α [°]	99.69(2)	99.51(2)	99.54(2)	99.555(6)	98.55(2)	98.46(1)	98.338(5)	98.27(1)	98.91(1)	98.746(8)	98.71(1)	98.54(2)
β [°]	114.98(2)	115.20(2)	115.24(2)	115.478(7)	115.68(2)	115.79(1)	115.953(5)	116.04(1)	115.41(1)	115.521(8)	115.61(1)	115.75(2)
γ [°]	98.38(2)	97.98(2)	97.99(2)	97.982(6)	99.58(1)	99.63(1)	99.690(5)	99.74(1)	99.50(1)	99.526(8)	99.56(1)	99.68(2)
V [Å^3]	2257.3(6)	2218.5(8)	2194.4(7)	2183.9(3)	2319.2(5)	2298.8(4)	2266.7(14)	2250.0(4)	2332.9(4)	2293.6(4)	2264.9(6)	2247.4(8)
$D_{calcd.}$ [g cm^{-3}]	1.514	1.540	1.557	1.565	1.600	1.615	1.638	1.650	1.717	1.747	1.769	1.783
μ (Mo-K_α) [mm^{-1}]	1.241	1.262	1.276	1.282	1.193	1.204	1.221	1.230	3.796	3.861	3.910	3.940
No. of collected refls.	22405	23958	23690	94870	23066	21904	27590	27229	23144	24197	68385	96901
No. of unique refls.	8278	14122	13968	16671	8548	8445	10195	10064	8570	14580	16363	17135
R(int)	0.1227	0.0921	0.1011	0.1405	0.0796	0.0610	0.0754	0.0645	0.0678	0.0973	0.1161	0.1535
R_1	0.0472	0.0499	0.0503	0.0520	0.0442	0.0419	0.0444	0.0419	0.0397	0.0551	0.0525	0.0512
wR_2	0.0911	0.0617	0.0620	0.0794	0.0759	0.0794	0.0867	0.0851	0.0653	0.0755	0.0841	0.0562
No. of parameters	515	515	515	515	543	543	543	543	543	543	543	543

Raman Spectroscopy: Raman measurements were performed with a Dilor XY micro-Raman (source: 632.8 nm line of a He-Ne laser; laser power density: ≈10^5 W cm^{-2}). The spectra were recorded at VV polarisation.

Mössbauer Spectroscopy: The variable-temperature Mössbauer measurements were obtained on a constant-acceleration spectrometer with a 50 mCi source of ^{57}Co (Rh matrix). The isomer shift values (δ) are given with respect to metallic iron at room temperature. The absorber was a sample of microcrystalline powder enclosed in a 2-cm-diameter cylindrical plastic sample holder, the size of which was determined to optimise the absorption. The variable-temperature spectra were obtained in the range 4.5–330 K using a He bath cryostat (Air Liquid DTA). Fitting parameters for all spectra were obtained by using a least-squares computer program.[48] The standard deviations of statistical origin are given in parentheses.

Supporting Information (see footnote on the first page of this article) contains four figures {magnetic behaviour of **1** with or without solvent, magnetic behaviour and magnetisation of [Fe(salten)-Mepepy][Ni(dmit)$_2$]$_3$, and Raman spectra of [Fe(salten)]Cl, [Fe(salten)Mepepy](BPh$_4$) and [Fe(salten)Mepepy][Ni(dmit)$_2$]} and seven tables (crystallographic data, geometrical data, short intermolecular distances and assignments of the Raman spectra).

Acknowledgments

The support and sponsorship of COST Action D14/0003/98 are acknowledged. S. D. thanks COST D14 for funding a Short Term Scientific Mission in Valencia.

[1] J. M. Williams, J. R. Ferraro, R. J. Thorn, K. D. Carlson, U. Geiser, H. H. Wang, A. M. Kini, M.-H. Whangbo, *Organic Superconductors (Including Fullerene): Synthesis Structure, Properties and Theory*, Prentice Hall, Englewood Cliff, NJ, **1992**.

[2] C. Faulmann, P. Cassoux, *Solid State Properties (Electronic, Magnetic, Optical) of Dithiolene Complex-based Compounds*, in *Progress in Inorganic Chemistry (Dithiolene Chemistry: Synthesis Properties, and Applications)* (Ed.: E. I Stiefel), John Wiley & Sons, Inc., **2004**, vol. 52, pp. 399–489.

[3] E. Coronado, P. Day, *Chem. Rev.* **2004**, *104*, 5419–5448.

[4] E. Coronado, J. R. Galán-Mascarós, *Inorg. Chem.* **2004**, *43*, 8072–8077.

[5] O. Margeat, P. G. Lacroix, J. P. Costes, B. Donnadieu, C. Lepetit, K. Nakatani, *Inorg. Chem.* **2004**, *43*, 4743–4750.

[6] E. Coronado, J. R. Galán-Mascarós, *J. Mater. Chem.* **2005**, *15*, 66–74.

[7] M. Kurmoo, A. W. Graham, P. Day, S. J. Coles, M. B. Hursthouse, J. L. Caufield, J. Singleton, F. L. Pratt, W. Hayes, L. Ducasse, P. Guionneau, *J. Am. Chem. Soc.* **1995**, *117*, 12209–12217.

[8] H. Kobayashi, A. Kobayashi, P. Cassoux, *Chem. Soc. Rev.* **2000**, *29*, 325–333.

[9] M. Tokumoto, T. Naito, H. Kobayashi, A. Kobayashi, V. N. Laukhin, L. Brossard, P. Cassoux, *Synth. Met.* **1997**, *86*, 2161–2162.

[10] A. Alberola, E. Coronado, J. R. Galan-Mascaros, C. Gimenez-Saiz, C. J. Gomez-Garcia, *J. Am. Chem. Soc.* **2003**, *125*, 10774–10775.

[11] A. Alberola, E. Coronado, J. R. Galan-Mascaros, C. Gimenez-Saiz, C. J. Gomez-Garcia, E. Martinez-Ferrero, A. Murcia-Martinez, *Synth. Met.* **2003**, *135–136*, 687–689.

[12] F. Setifi, L. Ouahab, S. Golhen, Y. Yoshida, G. Saito, *Inorg. Chem.* **2003**, *42*, 1791–1793.

[13] C. Faulmann, E. Riviere, S. Dorbes, F. Senocq, E. Coronado, P. Cassoux, *Eur. J. Inorg. Chem.* **2003**, 2880–2888.

[14] P. Gütlich, H. A. Goodwin, *Spin Crossover in Transition Metal Compounds I–III*, in *Topics in Current Chemistry*, **2004**; Vol. 233–235.

[15] P. J. van Koningsbruggen, Y. Maeda, H. Oshio, *Top. Curr. Chem.* **2004**, *233*, 259–324.

[16] S. Hayami, K. Inoue, S. Osaki, Y. Maeda, *Chem. Lett.* **1998**, 987–988.

[17] G. Juhasz, S. Hayami, O. Sato, Y. Maeda, *Chem. Phys. Lett.* **2002**, *364*, 164–170.

[18] S. Hayami, Z.-Z. Gu, M. Shiro, Y. Einaga, A. Fujishima, O. Sato, *J. Am. Chem. Soc.* **2000**, *122*, 11569.

[19] S. Dorbes, L. Valade, J. A. Real, C. Faulmann, *Chem. Commun.* **2005**, 69–71.

[20] S. Floquet, M.-L. Boillot, E. Riviere, F. Varret, K. Boukheddaden, D. Morineau, P. Negrier, *New J. Chem.* **2003**, *27*, 341–348.

[21] M. D. Timken, S. R. Wilson, D. N. Hendrickson, *Inorg. Chem.* **1985**, *24*, 3450.

[22] N. S. Gupta, M. Mohan, N. K. Jha, W. E. Antholine, *Inorg. Chim. Acta* **1991**, *184*, 13–21.
[23] M. S. Haddad, M. W. Lynch, W. D. Federer, D. N. Hendrickson, *Inorg. Chem.* **1981**, *20*, 123–131.
[24] F. V. Wells, S. W. McCann, H. H. Wickman, S. L. Kessel, D. N. Hendrickson, R. D. Feltham, *Inorg. Chem.* **1982**, *21*, 2306.
[25] A. Earnshaw, E. A. King, L. F. Larkworthy, *J. Chem. Soc. A* **1969**, 2459.
[26] H. Spiering, *Top. Curr. Chem.* **2004**, *235*, 171–195 and references cited therein.
[27] A. Sour, M.-L. Boillot, E. Riviere, P. Lesot, *Eur. J. Inorg. Chem.* **1999**, 2117–2119.
[28] An acetonitrile molecule was also found in the complex of Ni and its structure was solved at 160 K; it is similar to that of the Pd and Pt complexes (see Supporting Information for the X-ray data and CCDC-262733). Its magnetic properties are also similar to the properties of the Ni complex without solvent (see Supporting Information, Figure S1).
[29] A. E. Pullen, R. M. Olk, *Coord. Chem. Rev.* **1999**, *188*, 211–262.
[30] A. Bondi, *J. Phys. Chem.* **1964**, *68*, 441–451.
[31] G. N. Schrauzer, V. P. Mayweg, *J. Am. Chem. Soc.* **1965**, *87*, 3585–3592.
[32] R. M. Olk, R. Kirmse, E. Hoyer, C. Faulmann, P. Cassoux, *Z. Anorg. Allg. Chem.* **1994**, *620*, 90–100.
[33] K. I. Pokhodnya, C. Faulmann, I. Malfant, R. A. Solano, P. Cassoux, A. Mlayah, D. Smirnov, J. Leotin, *Synth. Met.* **1999**, *103*, 2016–2019.
[34] R. Boca, *Theoretical Foundations of Molecular Magnetism*, in *Current Methods in Inorganic Chemistry*, Elsevier, Amsterdam, **1999**; Vol. 1.
[35] A. Bousseksou, G. Molnár, G. G. Matouzenko, *Eur. J. Inorg. Chem.* **2004**, 4353–4369.
[36] A. Bousseksou, G. Molnar, *C. R. Chimie* **2003**, *6*, 1175–1183.
[37] N. N. Greenwood, T. C. Gibbs, *Mössbauer Spectroscopy,* Chapman Hall, New York, **1971**.
[38] M. Blume, *Phys. Rev.* **1968**, *174*, 351–358.
[39] J.-M. Vincent, S. Menage, J.-M. Latour, A. Bousseksou, J.-P. Tuchagues, A. Decian, M. Fontecave, *Angew. Chem. Int. Ed. Engl.* **1995**, *34*, 205–207.
[40] G. Steimecke, H. J. Sieler, R. Kirmse, E. Hoyer, *Phosphorus Sulfur* **1979**, *7*, 49–55.
[41] L. J. Farrugia, *J. Appl. Crystallogr.* **1999**, *32*, 837–838.
[42] A. Altomare, M. C. Burla, M. Camalli, G. L. Cascarano, C. Giacovazzo, A. Guagliardi, A. G. G. Moliterni, G. Polidori, R. Spagna, *J. Appl. Crystallogr.* **1999**, *32*, 115–119.
[43] G. M. Sheldrick *SHELXS97 – A Program for Automatic Solution of Crystal Structure (Release 97-2)*, University of Göttingen, Germany, **1997**.
[44] G. M. Sheldrick *SHELXL97 – Programs for Crystal Structure Analysis (Release 97-2)*, University of Göttingen, Germany, **1998**.
[45] A. L. Spek *PLATON, A Multipurpose Crystallographic Tool*, Utrecht University, Utrecht, The Netherlands, **1998**.
[46] *ORTEP3 for Windows*: L. J. Farrugia, *J. Appl. Crystallogr.* **1997**, *30*, 565.
[47] D. M. Watkin, L. Pearce, C. K. Prout *CAMERON – A Molecular Graphics Package*, Chemical Crystallography Laboratory, University of Oxford, **1993**.
[48] F. Varret, Indian National Science Academy, New Delhi, Jaipur, India, **1981**.

Received: February 10, 2005
Published Online: July 12, 2005

